GPCR and G protein mobility in D. discoideum : a single molecule study

Hemert, F. van

Chapter 4

RasC and RasG regulate membrane / cytoskeleton interactions which organize the polarized behavior of cAR1 and G$\beta\gamma$ in *D. discoideum*

D. discoideum expresses several Ras proteins of which 6 have been characterized. The proteins play roles in cytokinesis, growth, endocytosis en cell polarization. RasC and RasG are the best characterized Ras family-members and are the most important for motility and chemotaxis. The knockout phenotypes of both proteins include reduced random motility, loss of polarization, loss of cAMP relay, aberrant cytokinesis and chemotaxis. Nearly all effects except the defective cAMP-relay are a consequence of abnormal cytoskeleton structure and distribution. We showed before that the cytoskeleton plays a key role in several processes related to the dynamics of the GPCR / G-protein signaling cascade. The mobility of cAR1 is hindered by F-actin and the G$\beta\gamma$ subunit of the G protein immobilizes in a cAMP and leading edge specific manner. Here we report that in *rasC*$^{-}$*/rasG*$^{-}$ double knockout cells we don't

observe effects of actin on cAR1 diffusion. Moreover, there is no cAMP dependent immobilization of the Gβ subunit of the G-protein and no domains are formed. We conclude that RasC and RasG regulate F-actin / membrane interactions and membrane organization that are needed for proper cAR1 and Gβγ signaling in directional sensing.

4.1 Introduction

Dictyostelium discoideum is a widely used model organism for studying directed cell motility in chemical concentration gradients, a process called chemotaxis. Chemotaxis is part of more complex processes such as cytokinesis, wound healing and metastasis. *D. discoideum* shares considerable gene sequence homology with higher eukaryotes and many pathways are conserved both in protein homology and function between this amoeba and humans. Because of this fact and the modest culture requirements, its completely sequenced genome, and its accessibility to sensitive (single molecule) microscopy, *D. discoideum* is the organism of choice for many studies.

Chemotaxis is part of the *D. discoideum* lifecycle: upon starvation the cells change the expression of a number of genes resulting in the secretion of, and increased sensitivity to, cyclic adenosine mono-phosphate (cAMP). Within 24 hours the cells go through several stages of development including aggregation and the formation of a pseodoplasmodium (capable of phototaxis) which eventually culminates in a fruiting body used to disperse spores. In order to detect cAMP during the first stage of development, the cells use a G protein coupled receptor (GPCR) called cAMP receptor 1 (cAR1). The GPCR cAR1, upon binding of cAMP, promotes the exchange of guanine di-phosphate (GDP) for guanine tri-phosphate (GTP) in the Gα2 subunit of the Gα2βγ heterotrimer. Currently, evidence suggests that the activated Gα2 subunit (which has been shown to cycle between the cytosol and the membrane) shifts the balance in favor of the membrane and/or cAR1 bound state [22]. The Gβγ subunit detaches from the cAR1-Gα2 complex and immobilizes upon activation in an F-actin dependent manner, possibly as part of a feedback mechanism [22]. Among the most important downstream effectors of the G proteins are the Ras guanine exchange factors (RasGEFs). These proteins function as on switches for the

Ras family of small GTPases. Currently some of the putative RasGEFs have been investigated, for example *Aimless* which, when disrupted shows a phenotype combining the phenotypes of several Ras knockout lines [53]. Ras proteins are small, monomeric GTPases that can be toggled on or off. Just like the Gα subunits of heterotrimeric G proteins they cycle between an active GTP and an inactive GDP bound state [7]. While they are activated by RasGEFs, they are deactivated by Ras GTPase activating proteins (RasGAPs) [14]. Ras proteins are among the earliest molecules to show polarized activation [47, 79, 103]. In a cAMP gradient Ras stimulation leads to the polarized activation of PI3K [40, 30], phospholipase A2 (PLA2) [11], TorC2 and subsequently 2 PKB homologues (PKBA and PKBR1) [48]. Ultimately, the combined actions of these pathways result in orchestrated actin regulation that is required for efficient chemotaxis. *D. discoideum* has several Ras proteins of which RasC and RasG are the most important for chemotaxis [5].

Vegetative *rasC*- cells show reduced random motility, less polarization, altered F-actin distribution and are larger than wildtype (wt) cells [23]. These cells do not aggregate if left unattended. When pulsed with cAMP, or when mixed with wt cells they readily develop and move directionally towards a cAMP secreting micropipette suggesting a cAMP relay deficiency [61]. Major defects in the localization of myosin II, of F-actin organization, and a more general loss of cell polarity have been reported [95]. Although RasC and RasG have been shown to have overlapping functions, RasC is more important for adenylyl cyclase (ACA) activation whereas RasG is more important for directional movement [5].

The F-actin cytoskeleton in *D. discoideum* has a multitude of functions. It is used to maintain cell shape and to achieve polarity essential for development. Both processes require F-actin, but are different regarding their function and regulation. The F-actin in the cell cortex, important for the structural integrity of the cells, necessitates dynamic cross linking and active remodeling. At the leading edge of a highly mobile cell actin polymerizes at high rate and the growing polymers branch to prevent buckling [72]. Regulation does not go one way however. There are countless of examples in which F-actin or other cytoskeleton components regulate signaling [8, 94], and often there is a feedback between actin polymerization and the signaling controlling it [80, 42]. These feedback mechanisms may involve direct binding of

signaling proteins to actin [16] or may involve the physical mechanism of inhibition of protein mobility [94]. Thereby regulation of the interaction between actin and the cell membrane is of vital importance. The establishment of a differential cortex - membrane interaction in chemotacting cells may finally lead to amoeboid motion as pointed out by others [101, 58].

Previously we have shown that the mobility of cAR1 varies considerably upon latrunculin A (lat A) treatment and upon polarization of the cell, both indicative that cell cortex arrangement could be important for cAR1 function [17]. Moreover, the cortex - membrane interaction is polarized in chemtacting cells, as experimentally found in the reduced force that is required to aspirate the leading edge membrane compared to the trailing edge [64], and as an increase in cAR1 mobility specifically at the leading edge (chapter 3, [17]). In this paper we focus on the mobility of cAR1 and G$\beta\gamma$, both upstream regulators of Ras-signaling. Given that we have shown before that these two proteins interact with F-actin and the knowledge that RasC and RasG are major regulators of the F-actin cytoskeleton, we investigate here an internal feedback loop in signaling that is mediated by the polarized mobility of its components. Using a *rasC*$^{-}$/*rasG*$^{-}$ *D. discoideum* cell line, we probe the effects of disturbing this feedback loop on cAR1 and G$\beta\gamma$ mobility and activation.

4.2 Materials and methods

4.2.1 Cell culture

The JH10/*rasC*$^{-}$/*rasG*$^{-}$ cell line was kindly provided by Parvin Bolourani and created by transforming a *rasC-thy1* disruption vector into JH10 cells. Transformants were selected in the absence of thymidine [5]. Subsequently, the *rasC* disruption vector, pJLW26 [62] which carries a blasticidin resistance marker was transformed into the JH10/*rasG*$^{-}$ cells which were subsequently screened and selected [5]. We transformed these JH10/*rasC*$^{-}$/*rasG*$^{-}$ cells with a plasmid containing cAR1-eYFP or Gβ-eYFP and a G418 resistance marker using electroporation. The JH10/*rasC*$^{-}$/*rasG*$^{-}$ $\times$ cAR1-eYFP or Gβ-eYFP cells were cultured in 6 well plates containing HL-5c medium (Formedium) complemented with 10 µg/ml penicillin/streptomycin (1:1), 10 µg/ml blasticidin and 20 µg/ml G418 (Geneticin, Invitrogen).

4.2.2 Preparing naïve cells for measurements

A confluent 10 cm petridish was incubated overnight in low fluorescent medium (loflo, Formedium). In the morning, the cells were collected in 5 ml development buffer (DB, [24]) and washed by centrifugation for 4 min at a RCF of 400× g and then re-suspending in 5 ml fresh DB. The cells were subsequently incubated on the shaker (100 rpm) for 1 hr and then pulsed every 6 min with 150 nM final [cAMP] per pulse for 4 hr The cells were washed again and suspended in 5 ml fresh DB, shaken for another 40 min and left to settle for 20 min on the bottom of a 2-well chambered coverglass (Labtek). Cells that have not received any additional treatment are defined in the following as naïve.

4.2.3 Single molecule measurements

The experimental setup for single-molecule imaging has been described in detail previously [81]. The samples were mounted on an inverted microscope (Axiovert100, Zeiss) equipped with a 100× objective (NA=1.4, Zeiss). The region-of-interest on an ultrasensitive CCD camera coupled to the microscope was set to 50 × 50 pixels. The apparent pixelsize was 220 nm. Measurements were performed by illumination of the samples for 5 ms at 514 nm (Argon-ion laser, Spectra Physics) at an intensity of 2 kW/cm^2. The cells were photobleached for a period of 2-5 sec and sequences of 200-500 images with a timelag of 50 ms were taken. Use of an appropriate filter combination (Chroma) permitted the detection of the fluorescence signal on a liquid nitrogen-cooled CCD-camera (Princeton Instruments). The setup allowed us to image individual fluorophores at a signal-to-background-noise ratio of ∼30 leading to a positional accuracy of σ_0 = 40 nm. The measurements always focused on the apical cell membrane and never lasted longer than 15 - 60 sec per cell and 2 hr in total.

4.2.4 Global cAMP stimulation assay

After settling on the coverglass, the 1 ml DB that covered the cells was supplemented with cAMP to final concentration of 10 µM. Measurements commenced immediately and ended after 20 min involving ∼10-15 cells per experiment batch.

4.2.5 Applied gradient assay

By suspending a micropipette (Eppendorf femtotip) containing 10 µM cAMP just above the coverglass and applying a pressure of 40 KPa (pressure set by means of an Eppendorf Femtojet), a stable concentration gradient was created. The micropipette was placed at a distance of ∼70 µm from the cells creating a putative gradient of 4 nM/µm over the cells. This gradient was experimentally verified using a fluorescent dye in the pipette. The region of interest was 11 µm^2 which during measurement of the anterior and posterior of the cell body means that we observe ∼20% of the cell length.

4.2.6 Latrunculin A treatment

The cells were incubated in DB supplemented with 0.5 µM latrunculin A (Cayman Europe) for 10 min before the measurements began. Measurements were taken within 10 min.

4.2.7 Data analysis

Individual molecule positions were determined within each image in an image stack by fitting the signal intensity profiles to a 2D Gaussian function using Matlab (Mathworks Inc). The center of mass of the Gaussian fit corresponds within ∼40 nm to the single molecule positions. The latter were subsequently used to perform particle image correlation spectroscopy [83]. PICS calculates the 2-point correlation between individual molecule positions at two different times from which the cumulative distribution function of squared displacements ($cdf(r^2, tlag)$) for each timelag (t_{lag}) from 50-400 ms was constructed. The cdf's were fitted to a two fraction model:

$$cdf(r^2, t_{lag}) = 1 - \left(\alpha \cdot \exp\left(-\frac{r^2}{MSD_1}\right) + (1-\alpha)\exp\left(-\frac{r^2}{MSD_2}\right)\right) \quad (4.1)$$

The fast fraction size, α, was globally fitted over all timelags in each data set. This yielded 2 mean squared displacements (MSDs) per timelag and one fast fraction size for each data set. Subsequently the 2 MSDs are plotted versus t_{lag} resulting in

a representation of the mobility largely following that expected for diffusion. To determine the diffusion constant we fit each of the MSD *vs* time data to a free diffusion model:

$$MSD(t_{lag}) = 4Dt_{lag} + s_0 \tag{4.2}$$

This gives us the two diffusion constants (D_1 & D_2) and offsets (s_0) for each dataset. In the case that two dataset are compared (for example anterior *vs* posterior), MSD_1 and MSD_2 are kept equal per timelag for the two datasets and the fast fraction size, α, is kept constant per dataset resulting in 2 diffusion constants and two fraction sizes per fit. In this analysis, α is the only parameter left that characterizes the difference between two experimental conditions or two locations along the cell membrane.

The offset (s_0) is a representation of the accuracy by which the position of the molecules is determined. s_0 scales with the signal-to-noise-ratio of the single-molecule signal ($s_0 = 4\sigma^2$ = 0.0064 μm^2 with σ = 40 nm). It should be noted that not every observation yields the same signal-to-noise ratio, leading to a distribution of positional accuracies in each dataset. If s_0 approaches the mean-squared displacement of both fractions (as is the case for cAR1) and the appropriate fit of the data to (eq.4.1) fails. We have shown by simulation that this can be corrected for by allowing s_0 to be different for the two fractions in equation 4.2 (see Appendix chapter 3).

4.3 Results

Using wide-field single-molecule fluorescence microscopy (fig.4.1, bottom left), individual cAR1-eYFP and Gβγ-eYFP molecules diffusing in the membrane of living *D. discoideum* cells are visualized (fig.4.1, bottom right). The data consists of image stacks (typical 500 images) from which the positions of molecules at specific time points are determined by Gaussian fitting to an accuracy of 40 nm. Typically 2-6 $\cdot 10^4$ positions obtained from the observation of 40-100 cells are used for analysis. Particle image correlation-spectroscopy (PICS [83]) is applied to calculate the correlation between the positions of the molecules in two images at each timelag which results in the cumulative probability of the squared displacements (cdf) for the time-

lag between the images (typically 50-400 ms). All cdfs related to the current work are found in the supplemetal materials. The cdfs are subsequently fit to two distinct mobility fractions characterized by the mean squared displacement of a fast (MSD_1) and a slow (MSD_2) component, and a fraction size of the fast component, α. The slope of the MSDs *vs* time lag represents the diffusion constant that characterizes protein mobility in the membrane (fig.4.1, bottom right). The result of such detailed mobility analysis of cAR1 in naïve wt cells is shown in figure 4.1 (bottom right). As predicted for free diffusion the MSDs of both fractions scale linearly with timelag characterized by diffusion constants of $D_1 = 0.015 \pm 0.002$ μm^2/s and $D_2 = 0.007 \pm 0.001$ μm^2/s for the fast and slow fraction, respectively. Thereby $\alpha = 0.45 \pm 0.06$ of the population is contained in the fast fraction. In the subsequent figures this result on naïve cells is indicated as dotted black line.

4.3.1 The mobility of cAR1 in *rasC*$^-$/*rasG*$^-$ cells is increased and reflects the mobility found for F-actin depleted cells

We have shown before that the mobility of cAR1 depends on the presence of an intact cell cortex. Disruption of the cell cytoskeleton by lat A treatment resulted in an increased cAR1 mobility (chapter 3). Presumably membrane localized molecules are hindered in their mobility due to the presence of F-actin filaments directly (fence model), or by trans-membrane proteins that are attached to the filaments (picket fence model [29, 86]). We studied cAR1 mobility in a *rasC*$^-$/*rasG*$^-$ double knockout background (JH10/*rasC*$^-$/*rasG*$^-$). These cells were reported to show disregulation of their cytoskeleton meshwork [5].

In a *rasC*$^-$/*rasG*$^-$ cells we found the mobility of cAR1 to be increased with respect to naïve wt cells (fig.4.1, bottom right and fig.4.2, black dotted line). The overall cAR1 mobility matched that of cAR1 in cells that are treated with 0.5 μM latrunculin A (fig.4.2, green dotted line), indicative of reduced cortex strength or less tight cortex - membrane interactions. In comparison to wt naïve cells the diffusion constant of the fast fraction increased twofold to $D_1 = 0.029 \pm 0.002$ μm^2/s and that of the slow fraction to $D_2 = 0.012 \pm 0.002$ μm^2/s. Simultaneously the size of the fast fraction dropped to $\alpha = 0.30 \pm 0.10$. All three parameters representing cAR1 mobility are comparable to those found for lat A treated naïve wt cells ($D_1 = 0.028$

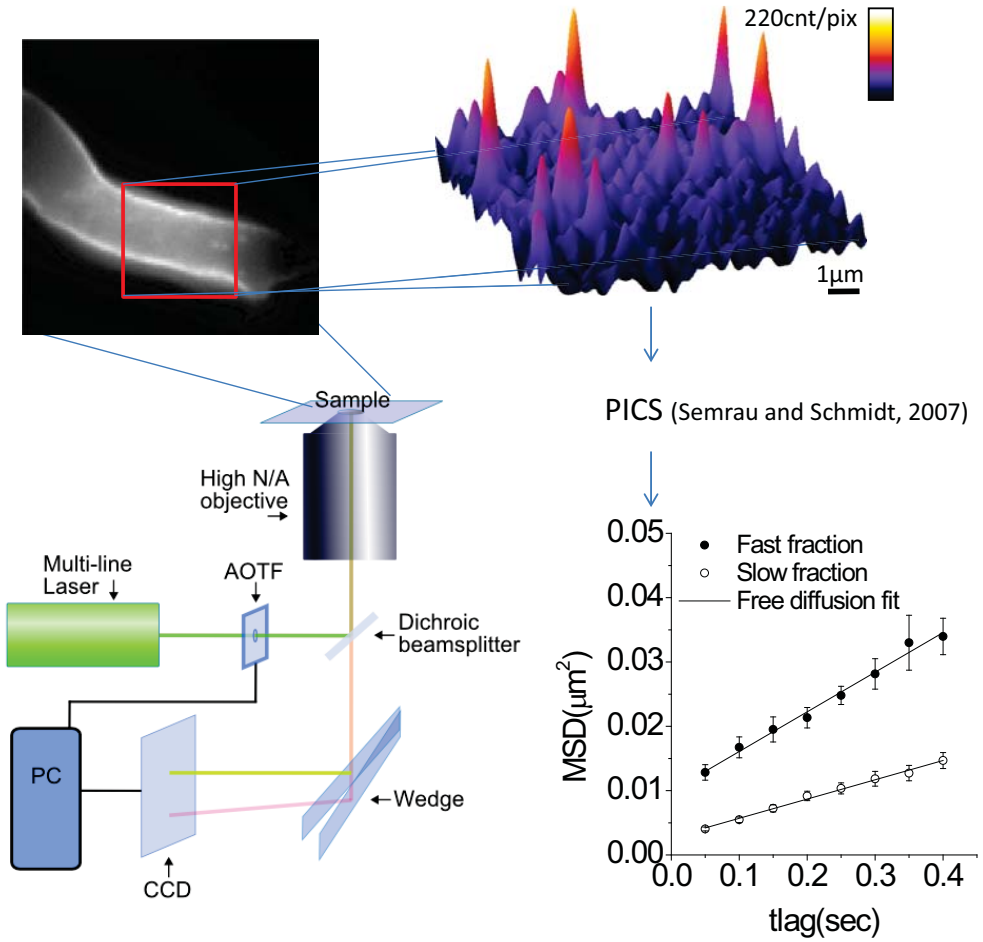

Figure 4.1: Description of the technique and data acquisition. Images of individual cAR1-eYFP and Gβ-eYFP molecules at the apical membrane of *D.discoideum* cells are taken at a rate of 20 Hz on an inverted microscope (bottom left). Individual molecule signals are identified and their position determined with an accuracy of ∼40 nm (top right). The position information is used in particle image correlation-spectroscopy to construct the cumulative density functions (cdfs) of squared displacements (see supplemental figures) over timelags ranging from 50 to 400 ms. Fitting of a bi-exponential and a global fraction size (eq.4.1, section 4.2) results in two diffusion constants and a fraction size of the fast component. For the mobility of cAR1 in naive wt cells $D_1 = 0.015 \pm 0.002$ µm^2/s, $D_2 = 0.007 \pm 0.001$ µm^2/s, and $\alpha = 0.45 \pm 0.06$ (bottom right).

$\pm$ 0.006 μm^2/s, D_2 = 0.015 $\pm$ 0.002 μm^2/s, and α = 0.37 $\pm$ 0.06 (chapter 3)).

Whether the increased mobility of cAR1 in the *rasC*$^-$/*rasG*$^-$ cells is due to aberrant regulation of the F-actin cytoskeleton or to direct interaction between cAR1 and Ras was investigated by additional treatment of the cells with latrunculin A (lat A). In the first case lat A treatment should not affect the cAR1 mobility whereas in the latter lat A treatment should lead to a further increase of cAR1 mobility.

The mobility of cAR1 was unchanged after treatment of *rasC*$^-$/*rasG*$^-$ cells with lat A (see the cdfs in supplemental figure 4.7) for *rasC*$^-$/*rasG*$^-$, in contrast to wt cells receiving the same treatment (fig.4.8). For this reason we analyze the data assuming the mobility for both fractions is equal and leave the fraction size (α) as the only free parameter across the datasets (fig.4.3). This analysis yields D_1 = 0.029 $\pm$ 0.002 μm^2/s and D_2 = 0.012 $\pm$ 0.002 μm^2/s for the fast and slow fractions, respectively. The size of the fast fraction after lat A treatment is α = 0.35 $\pm$ 0.11, equivalent to that of untreated *rasC*$^-$/*rasG*$^-$ cells (where α = 0.30 $\pm$ 0.10). As an internal check we also analyzed wt cells before and after lat A treatment in the same way, which leads to a difference in fraction size of $\Delta\alpha$ = 0.37 (data not shown).

4.3.2 The polarized mobility of cAR1 is lost in the *rasC*$^-$/*rasG*$^-$ knockout

It was reported before [5] that naïve *rasC*$^-$/*rasG*$^-$ double knockout cells do not move directionally. After transformation with cAR1-eYFP however the *rasC*$^-$/*rasG*$^-$ cells attain elongated shapes and are able to move directionally towards a cAMP secreting micropipette (fig.4.4 and fig.4.10A) albeit without forming stream as the wt cells do (fig.4.10B). The fact that introduction of cAR1 restores directional sensing is expected since *carA* (the cAR1 gene) is among the genes whose expression is virtually absent in the *rasC*$^-$/*rasG*$^-$ cells [5] and a functional cAR1 molecule is required for the activation of genes leading to aggregation [50].

In wt cells that are polarized in a cAMP gradient we reported before that the mobility of cAR1 is polarized and characterized by an increased size of the fast fraction by $\Delta\alpha$ 0.23 at the leading edge of the cell [17]. We speculated that this increased mobile fraction would lead to an initial amplification of the external signal towards downstream effectors. Further we found that polarization in cAR1 mobility was in-

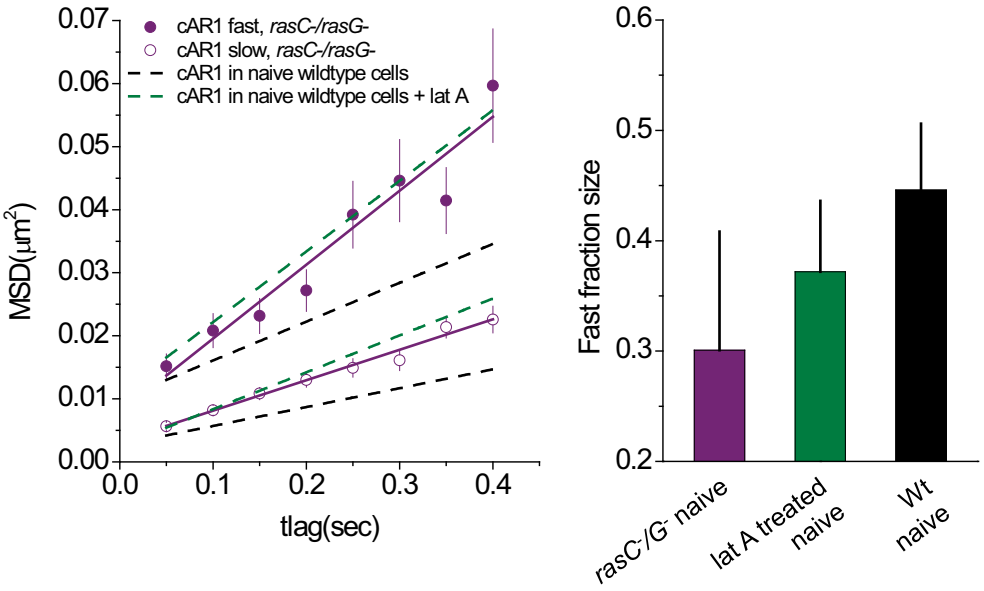

Figure 4.2: cAR1 mobility is elevated in *rasC*$^-$*/rasG*$^-$ cells. The *rasC*$^-$*/rasG*$^-$ cells have very amorphous shapes, much more so as wt cells (not shown). The membrane shows thick knob like structures as well as very long (>10 µM) and thin filopodia. The filopodia are found all over the glass slide and often appear to extend from the back of moving cells. When we compare the MSD *vs* time lag behavior of cAR1 in the *rasC*$^-$*/rasG*$^-$ cells (purple circles/line) to that of cAR1 in naïve wt cells (black dotted line) a twofold increased mobility is observed in both fractions. The fast fraction increases its diffusion constant from $D_1 = 0.015 \pm 0.002$ µm^2/s to$D_1 = 0.028 \pm 0.007$ µm^2/s whereas the slow fraction goes from $D_2 = 0.007 \pm 0.001$ µm^2/s to $D_2 = 0.012 \pm 0.001$ µm^2/s in the absence of RasC and RasG. The cAR1 molecules in this mutant show the same behavior as cAR1 in lat A treated wt cells ($D_1 = 0.028 \pm 0.006$ µm^2/s and $D_2 = 0.015 \pm 0.002$ µm^2/s). The fast fraction sizes do not differ significantly (α in equation 4.1).

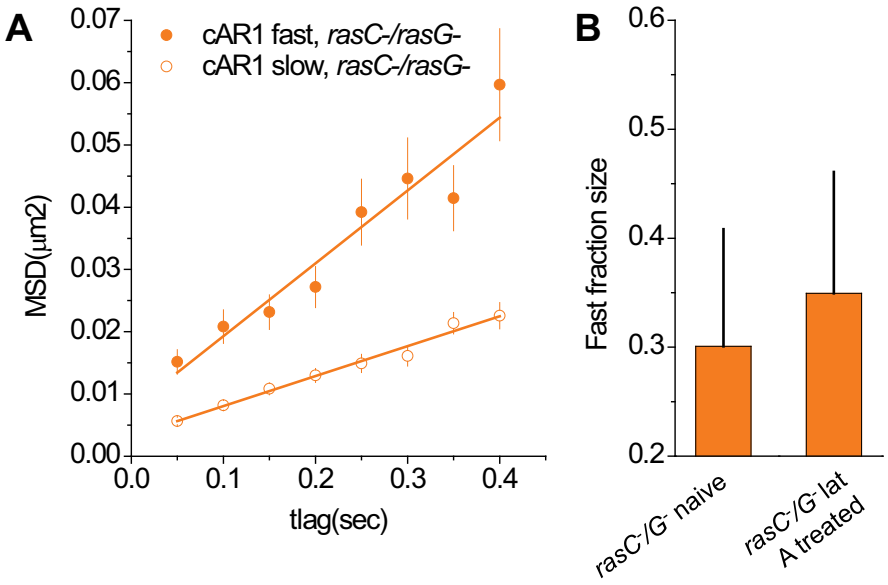

Figure 4.3: F-actin does not obstruct cAR1 diffusion in *rasC*$^{-}$/*rasG*$^{-}$ cells. The mobility of cAR1 in lat A treated *rasC*$^{-}$/*rasG*$^{-}$ cells was compared to untreated cells by means of keeping the MSDs equal for each time lag and comparing the globally fitted fast fraction sizes. In contrast to wt cells which undergo lat A treatment, in *rasC*$^{-}$/*rasG*$^{-}$ cells, the mobility does not increase significantly.

dependent of F-actin breakdown (chapter 3) together suggesting that F-actin plays a role in cAR1 mobility, but does not influence the development of cellular polarity.

Given the results on cAR1 mobility in *rasC*$^{-}$*/rasG*$^{-}$ cells shown above, which suggest that the F-actin cortex in those cells is heavily compromised, we would predict that a polarized mobility behavior would evolve in *rasC*$^{-}$*/rasG*$^{-}$ cells since we showed that this polarization was F-actin independent. Surprisingly, we did not observe any difference between the anterior and the posterior regarding cAR1 mobility in *rasC*$^{-}$*/rasG*$^{-}$ (fig.4.4 and fig.4.9). The mobility as characterized by D_1 = 0.029 $\pm$ 0.002 $\mu m^2/s$, D_2 = 0.010 $\pm$ 0.001 $\mu m^2/s$, and $\alpha_{anterior}$ = 0.34 $\pm$ 0.25 *vs* $\alpha_{posterior}$ = 0.33 $\pm$ 0.25 is not different from the mobility measured in naïve *rasC*$^{-}$*/rasG*$^{-}$ or lat A treated wt cells. Apparently, the cortex rearrangements resulting in higher anterior cAR1 mobility that take place in polarized wt cells do not take place in *rasC*$^{-}$*/rasG*$^{-}$ cells, that includes the F-actin independent interactions reported before (chapter 3).

4.3.3 G$\beta\gamma$ in the RasC/RasG knockout does not immobilize upon cAMP stimulation

In parallel to the polarized cAR1 mobility we have reported before on a cAMP, anterior specific and F-actin dependent immobilization of the G$\beta\gamma$ subunit of the G protein upon activation of cAR1. We hypothesized that this immobilization may be important for downstream signaling by G$\beta\gamma$ and might help the cell in forming a persistent leading edge using a G$\beta\gamma$ - F actin feedback loop. We were curious to see whether the abolishing of RasG and RasC signaling would also abolish this interaction loop.

Before cAMP stimulation the mobility of G$\beta\gamma$ in *rasC*$^{-}$*/rasG*$^{-}$ (fig.4.5, yellow dots) was indistinguishable from that in wt cells (black dotted line) characterized by D_1 = 0.11 $\pm$ 0.01 $\mu m^2/s$, D_2 = 0.013 $\pm$ 0.005 $\mu m^2/s$, and α = 0.67 $\pm$ 0.06. It is worth noting that the slow fraction of G$\beta\gamma$ still shows the same diffusivity as a fraction of the cAR1 molecules (fig.4.5B and fig.4.1, bottom right) suggesting that part of the receptors are precoupled to the G protein prior to stimulation. Upon activation, in contrast to wt cells, no change in mobility of G$\beta\gamma$ was observed. In the presence of cAMP the diffusion is characterized by D_1 = 0.12 $\pm$ 0.01 $\mu m^2/s$, D_2 = 0.015 $\pm$ 0.006 $\mu m^2/s$, and α = 0.73 $\pm$ 0.08.

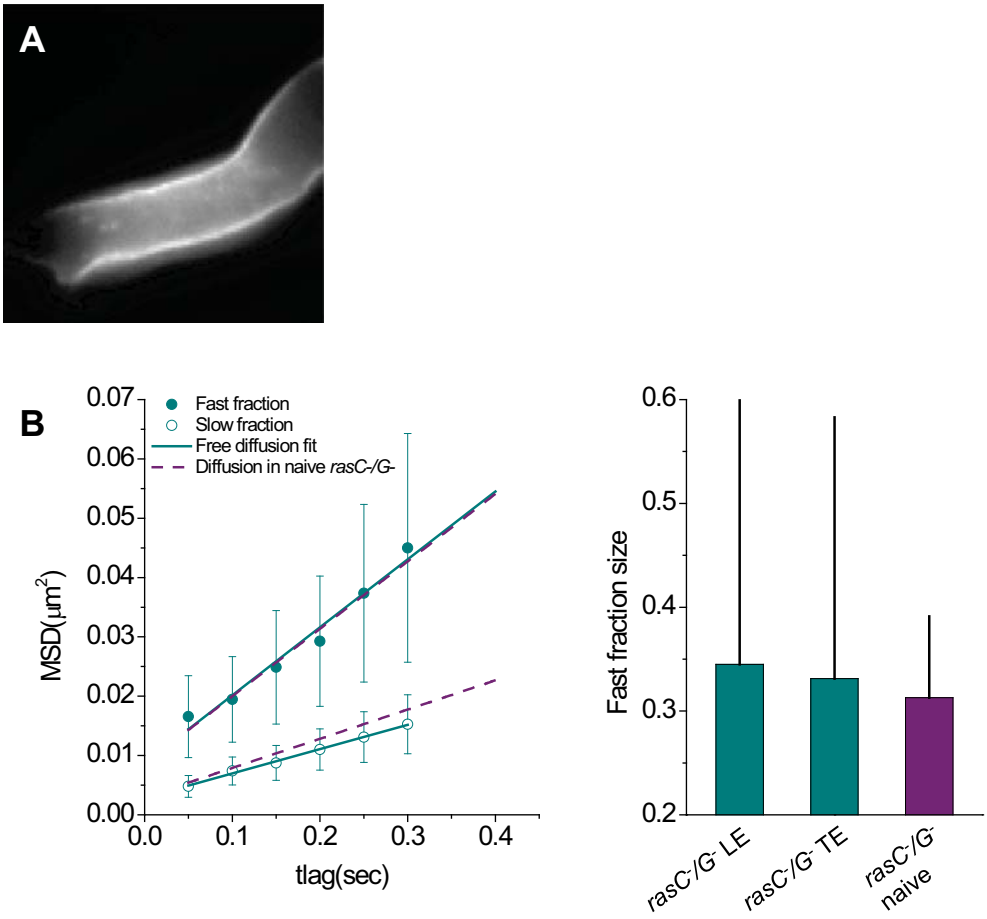

Figure 4.4: The increased mobility of cAR1 and the anterior mobility shift during chemotaxis are lost in the *rasC⁻/rasG⁻* cells. **(A)** The *rasC⁻/rasG⁻* × cAR1-eYFP cells were subjected to a chemotactic needle assay. As suggested earlier, introduction of a functional cAR1 rescues the chemotaxis defects of the *rasC⁻/rasG⁻* cells [5]. The cells polarized (poorly) and crawled directionally to the needle (fig.4.10A). The mobility at the anterior was compared to the posterior, again by leaving the fast fraction size as the only parameter that defines the overall mobility difference between the two datasets. There is no difference in cAR1 mobility between the leading and trailing edge. Moreover, the diffusion of the fitted slow and fast fractions were found to be $D_1 = 0.029 \pm 0.002$ μm^2/s and $D_2 = 0.010 \pm 0.002$ μm^2/s which does not differ from the mobility in naïve *rasC⁻/rasG⁻* and the lat A treated wt cells.

Not surprisingly the F-actin dependent microdomains which obstructed the diffusion of the fast fraction disappeared (fig.4.5C). Also the complete immobilization of the slow fraction of G$\beta\gamma$ did not appear (fig.4.5D) which is readily explained by the disrupted F-actin cortex in *rasC$^-$/rasG$^-$*. More importantly however was the disappearance of the characteristic increase in slow fraction size observed in wt cells (fig.4.5E) that characterized cellular polarity independent of F-actin (chapter 2) which suggests that this event is not a direct result of Gβ activation as suggested earlier but of something downstream of RasC and RasG and upstream of F-actin.

4.4 Discussion

Previously we have shown that the mobility characteristics of both the G protein coupled receptor cAR1 and its associated G protein heterotrimer, G$\alpha 2\beta\gamma$, are influenced by F-actin. We hypothesized that this interaction plays a role in an F-actin/cAR1/G protein feedback mechanism that might rely on the temporal enclosement or slowdown of the proteins into signaling domains, a process which has been heavily discussed in literature [55]. Since F-actin organization depends highly on the Ras family of small GTPases, specifically RasC and RasG, we investigated cAR1 and G$\beta\gamma$ dynamics in a *rasC$^-$/rasG$^-$ D. discoideum* cell line in order to unravel correlations between protein mobility and biological function.

The *rasC$^-$/rasG$^-$ D. discoideum* cell line was shown before to be virtually deficient in chemotactic signaling [5]. In a chemotaxis needle assay these cells, when transformed with functional cAR1, did move towards the needle albeit at heavily reduced efficiency (fig.4.10A) as compared to wt cells (fig.4.10B) and without forming streams. As briefly touched upon in the results section, this is probably explained by the fact that we introduce a functional cAR1. It was shown that cAR1 is vital to the expression of proteins important for development [50]. Our results suggest that the lack of directed cell movement may be the direct result of the absence of cAR1 expression in the *rasC$^-$/rasG$^-$* cells as Bolourani et al. also suggested [5].

We show here that the mobility of cAR1 in naïve RasC/RasG knockout cells is similar to that in naïve wt cells treated with lat A. When *rasC$^-$/rasG$^-$* cells experience a cAMP gradient, however, they do not show any polarized behavior in terms of

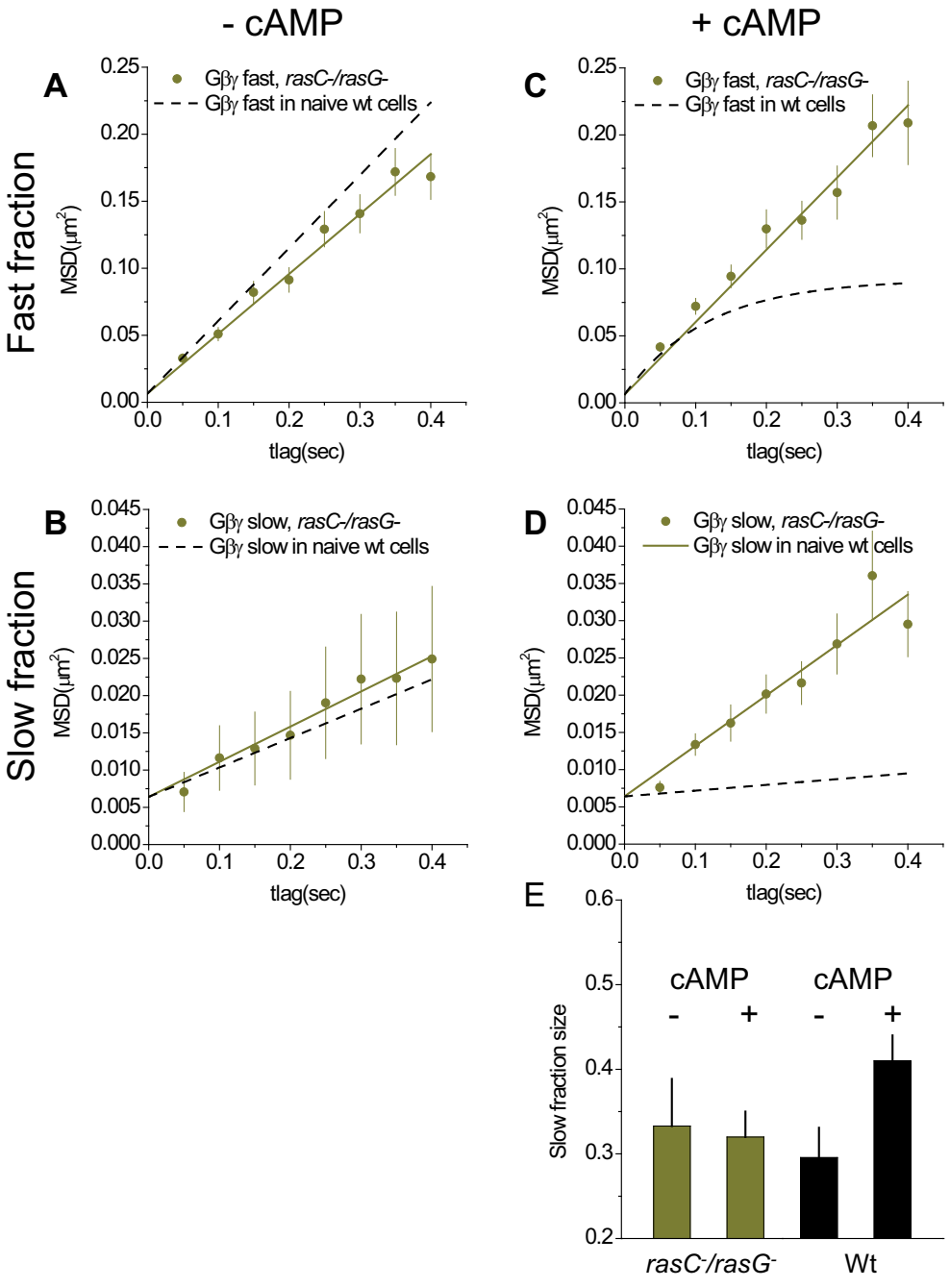
- cAMP
+ cAMP
Fast fraction
Slow fraction
A
B
C
D
E
Gβγ fast, rasC-/rasG-
Gβγ fast in naive wt cells
Gβγ fast in wt cells
Gβγ slow, rasC-/rasG-
Gβγ slow in naive wt cells
MSD(μm²)
tlag(sec)
Slow fraction size
cAMP
-
+
rasC-/rasG-
Wt

Figure 4.5: G$\beta\gamma$ does not immobilize and membrane micro domains do not form upon global cAMP stimulation of the *rasC$^-$/rasG$^-$* cells. **(A)** In naïve *rasC$^-$/rasG$^-$* cells the mobility of the fast fraction of G$\beta\gamma$ (yellow points) resembles that in naïve wt cells (black dotted line). **(B)** This is also true for the slow fraction. **(C)** Upon addition of 10 µM cAMP to wt cells F-actin dependent confined diffusion is observed (black dotted line), an effect which doesn't take place in the *rasC$^-$/rasG$^-$* cells (yellow points). **(D)** The slow fraction in wt cells immobilizes (black dotted line), an effect which requires F-actin polymerization and intact RasC/RasG signaling (yellow points). **(E)** The characteristic increase in slow fraction size was observed upon global cAMP stimulation of wt cells (black bars). This effect was shown to be F-actin independent (chapter 3), the effect is lost in the RasC/RasG knockout cell line (yellow bars).

cAR1 and G$\beta\gamma$ mobility. In contrast, wt cells which were treated by lat A to break down the cytoskeleton still exhibit polarized cAR1 mobility (chapter 3). Likewise, the immobilization of G$\beta\gamma$ upon cAMP activation (chapter 2) which was found to be cAMP, cAR1, Gα2 and F-actin dependent, does not occur in *rasC*$^{-}$/*rasG*$^{-}$ cells.

The close resemblance of cAR1 mobility in *rasC*$^{-}$/*rasG*$^{-}$ to that found in naïve wt cells upon treatment with lat A (fig.4.2; chapter 3) can be indicative of either i; reduced F-actin polymerization in the absence of RasC and RasG, ii; RasC and RasG directly mediate cAR1 binding to F-actin, or iii; RasC and RasG are required for the interaction of F-actin with the membrane. Given the fact that the *rasG*$^{-}$ cells have similar amounts of F-actin [88] and *rasC*$^{-}$ only shows deficiencies in down-regulating actin polymerization at the back of a cAMP wave [95], hypothesis i seems unlikely. We can't disprove the second hypothesis (ii) here, although a direct interaction between cAR1 and the Ras proteins seems unlikely, such an interaction would facilitate rapid activation of Ras by precoupled G-proteins. Given the fact that the RasG/RasC knockout phenotype includes countless F-actin related deficiencies hypothesis iii seems most probable as the interpretation of our results. Probably RasC and RasG are important regulators for the local membrane organization that is predicted for proper functioning of the complex signaling networks in cells [55].

The fact that we don't find any effect on the mobility of cAR1 upon lat A treatment of the *rasC*$^{-}$/*rasG*$^{-}$ cells compared to a significant effect in wt cells ($\Delta\alpha = 6\%$ *vs* $\Delta\alpha = 37\%$, respectively) further supports the hypothesis that RasC and RasG play a role in the F-actin - membrane interaction. This interaction can be either direct, e.g.: RasC or RasG actively couples F-actin to the membrane, or indirect, e.g.: in the absence of RasC or RasG F-actin organizes in such a way that a tight interaction with the membrane is disturbed. Since Ras proteins are upstream of myosin II regulation both at the cells anterior and posterior [53] and myosin is a principal F-actin regulator, this is a likely explanation.

The most striking finding in *rasC*$^{-}$/*rasG*$^{-}$ cells is the loss of polarized mobility of cAR1 in a gradient of cAMP. In an earlier paper we attributed the polarized mobility of cAR1 to differential cortex - membrane interactions although other factors also contribute (chapter 3). As we show here, the *rasC*$^{-}$/*rasG*$^{-}$ mutant has a cortex defect affecting cAR1 mobility. Because RasC and RasG are important regulators

of F-actin dynamics, we expected to see the same result as in lat A treated wt cells namely, prevalence of the polarized mobility regarding cAR1. However, the mobility between the anterior and posterior of *rasC*$^-$*/rasG*$^-$ cells in a cAMP gradient did not differ indicating that factors that influence the cortex, membrane or cortex - membrane interactions other then F-actin influence cAR1 mobility, as we already suggested. These factors are downstream of RasC/RasG and involved in gradient sensing. Possible candidates are signaling membrane lipids (PI(3,4,5)P_3/PI(4,5)P_2) and/or cortex components other then F-actin. Our speculation of differential cortex - membrane interactions was backed by the fact that lat A treatment globally increased cAR1 mobility (chapter 3). Furthermore, micropipette aspiration experiments that locally probe the elastic properties of the membrane showed a smaller elastic constant of the anterior membrane as compared to the posterior membrane [64]. It was shown that leading edge specific breakdown of the cortex is part of an alternative method of amoeboid movement [101]. Hence, it seems that the *rasC*$^-$*/rasG*$^-$ cells are not capable of modulating cortex strength in a spatial manner that might be needed for proper cellular signaling and locomotion. This further suggests that *rasC*$^-$*/rasG*$^-$ will be deficient in discriminating anterior and posterior with regard to the cortex which might well be the cause of their inefficient random and directed movement.

The latter hypothesis was confirmed by experiments on G$\beta\gamma$ mobility. The fact that we do not observe immobilization of G$\beta\gamma$ in *rasC*$^-$*/rasG*$^-$ came as a surprise. The *rasC*$^-$*/rasG*$^-$ cells are certainly not deprived of F-actin [88] but only show aberrant mechanical properties [95]. The fact that G$\beta\gamma$ does not immobilize upon activation suggests either a physical difference between the F-actin in *rasC*$^-$*/rasG*$^-$ and that in wt cells or lack of a so far not identified G$\beta\gamma$ - F-actin binding factor which could be either RasC or RasG. If this were to be the case, we are able to explain leading edge specific G$\beta\gamma$ immobilization a as result of the local Ras activation [47, 79].

In conclusion our findings support the fact that RasC and RasG are important for actin dynamics but also suggest a function in regulating F-actin - membrane interactions. RasC and RasG appear to play a role in organizing the local membrane structure such that activation remains localized and pseudopods are stabilized (fig.4.6). The former are concluded from our finding that Ras seems to be important for the G$\beta\gamma$ - F-actin binding we observed earlier, and thus for the suggested lead-

ing edge specific feedback mechanism. This hypothesis is supported by the fact that RasC/RasG knockout cells show reduced random movement [5]. The deficiency in proper membrane organization may finally lead to a deficiency in keeping activation localized, a hypothesis which will have to be tested in further experiments. We have shown that even though Ras is a downstream effector of cAR1 and the G protein, due to its influence on F-actin it indirectly alters the behavior of the two. Our results point towards a feedback mechanism between F-actin and the GPCR signaling involving Ras, the results might be applicable to a wide range of GPCR - G protein systems.

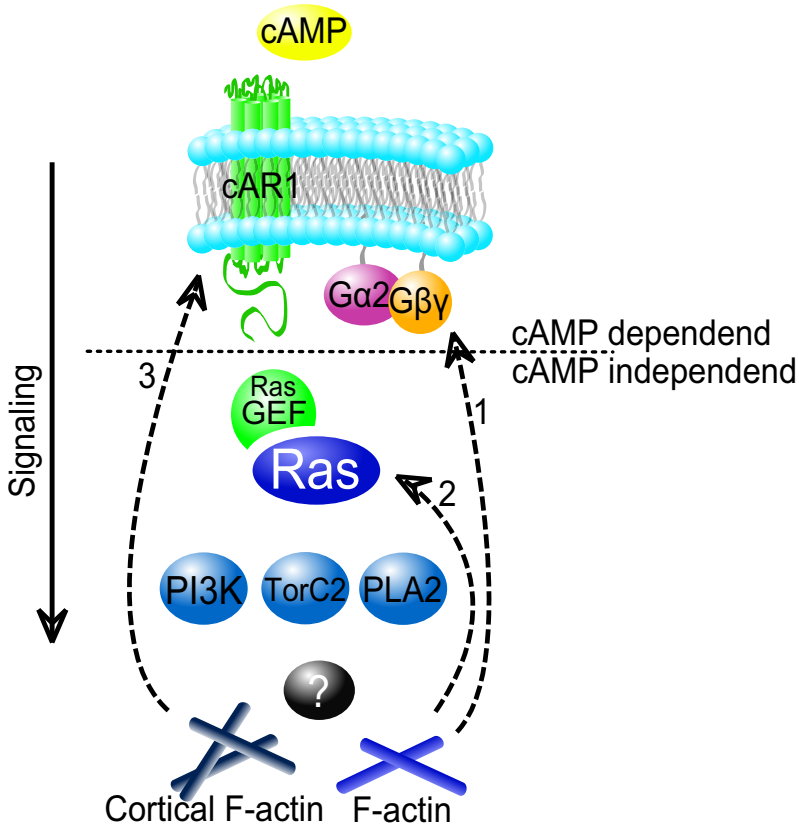

Figure 4.6: A model incorporating the results. Upon addition of cAMP to the cells, cAR1 is activated. The G protein heterotrimer splits into its $\alpha 2$ and $\beta\gamma$ subunit. RasGEFs are stimulated by the G protein and in turn function as on switches for the Ras family of small G proteins. Ras proteins then activate several downstream effectors for which it is currently unknown how they exactly lead to actin polymerization. This model incorporates several feedback mechanisms: 1; G$\beta\gamma$ immobilizes in a cAMP, cAR1, G$\alpha 2$, RasC/RasG and F-actin dependent manner. This immobilization also takes place specifically at the leading edge of a chemotaxing cell. We hypothesize that this specific F-actin - G$\beta\gamma$ interaction may function as an enhancer for G protein signaling and thus plays a role as a maintainer/amplifier of polarized chemotactic signaling. The F-actin independent but RasC/RasG dependent increase in slow fraction size upon activation however plays a part in gradient sensing. 2; A cAR1/G protein independent feedback mechanism has been suggested to exist between F-actin and members of the Ras family [80]. This mechanism helps to control stochastic changes in the cytoskeleton by stabilizing forming pseudopods, possibly the cause for reduced motility of the *rasC*$^{-}$*/rasG*$^{-}$ cells. 3; We have reported before that the diffusion speed of cAR1 is dominated by F-actin interactions (chapter 3) and that differential membrane cortex interactions may be responsible for the fact that cAR1 mobility is higher at the leading edge with respect to the trailing edge. We have shown in this paper that the regulation of cAR1 mobility by F-actin is Ras dependent but it does not require a functional G protein (chapter 3). Maintaining polarized cortex - membrane interactions however requires G protein and Ras signaling, consistent with idea that the Ras/PI3K/F-actin feedback mechanism does not require GPCR input whereas directed motion does.

Supplemental information

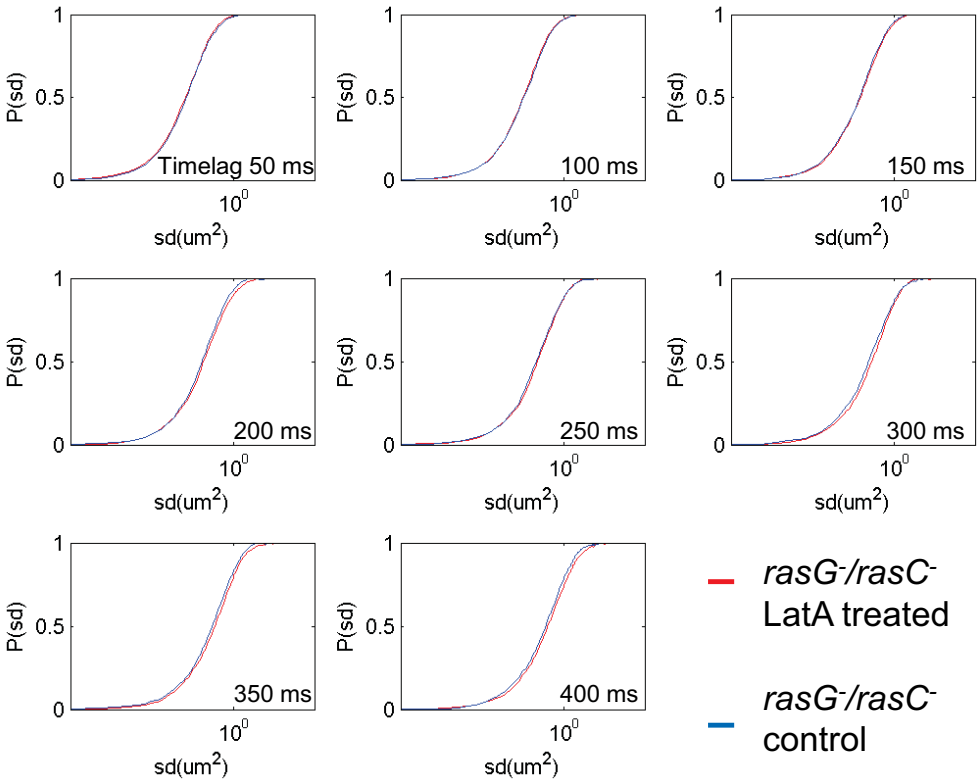

Figure 4.7: The mobility of cAR1 is equal in naïve and lat A treated in *rasC*$^{-}$/*rasG*$^{-}$ cells.

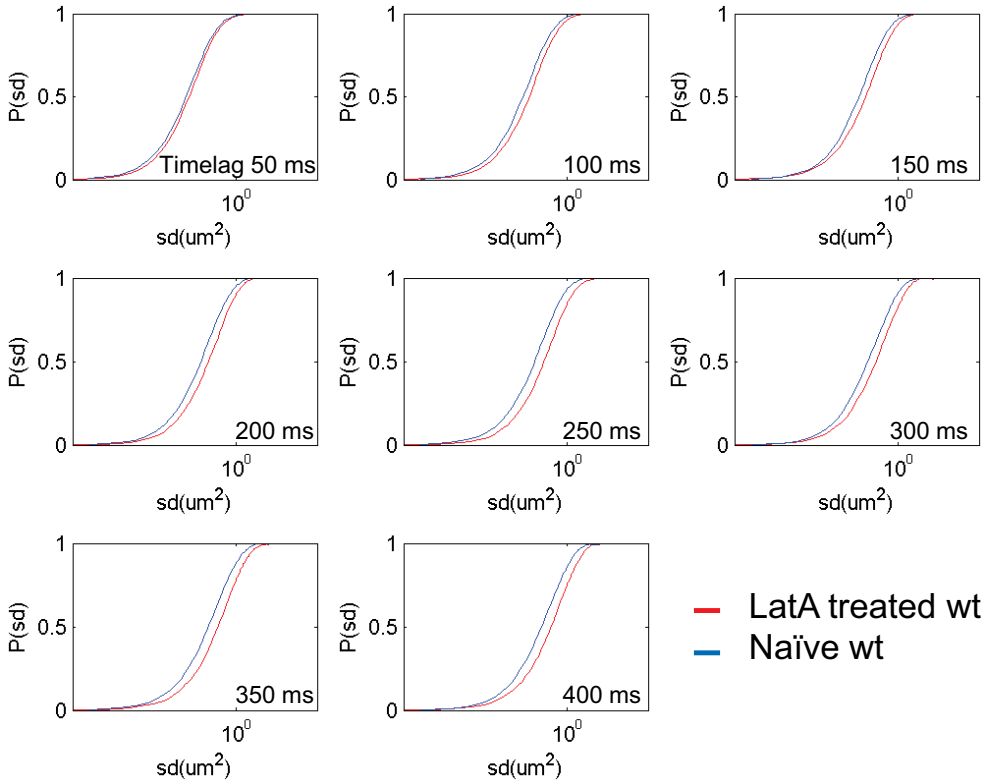

Figure 4.8: The mobility of cAR1 in wt cells is dramatically increased upon lat A treatment.

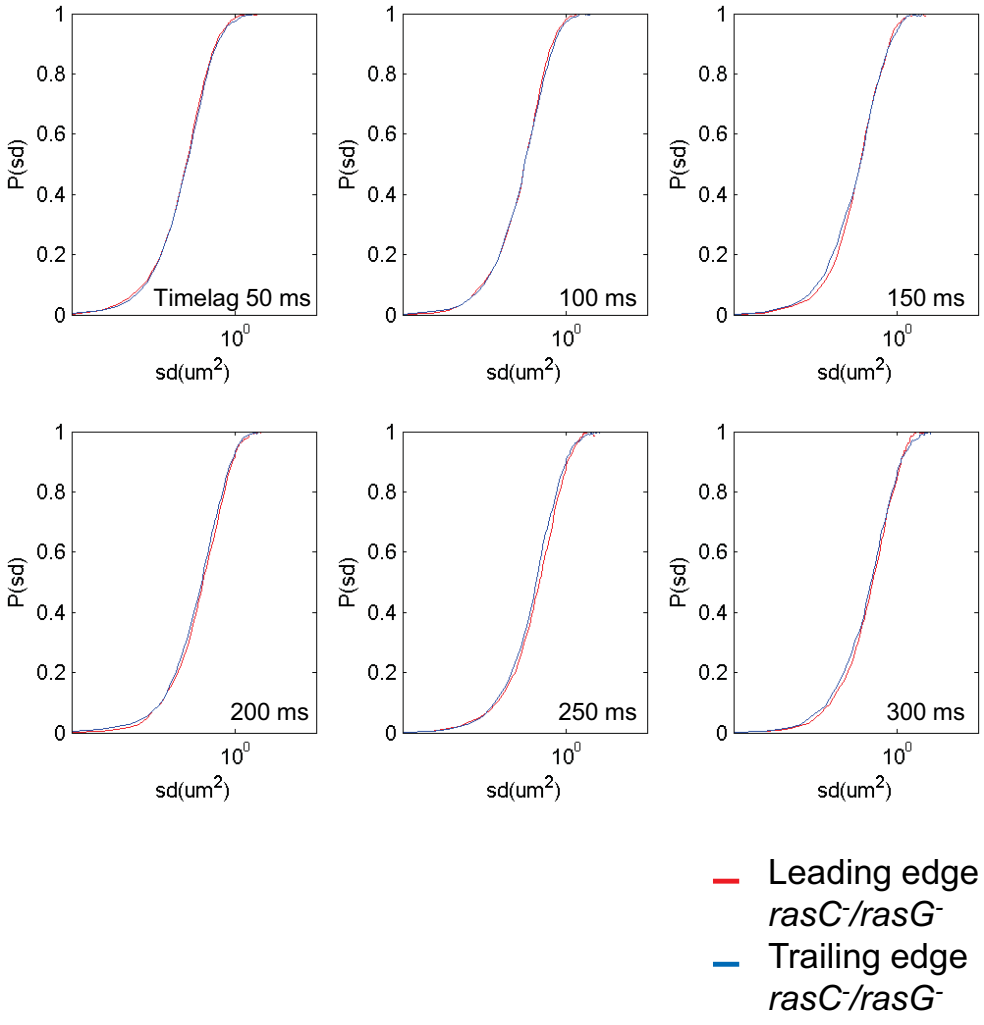

Figure 4.9: the mobility of cAR1 in chemotaxing *rasC*$^{-}$/*rasG*$^{-}$ is not polarized.

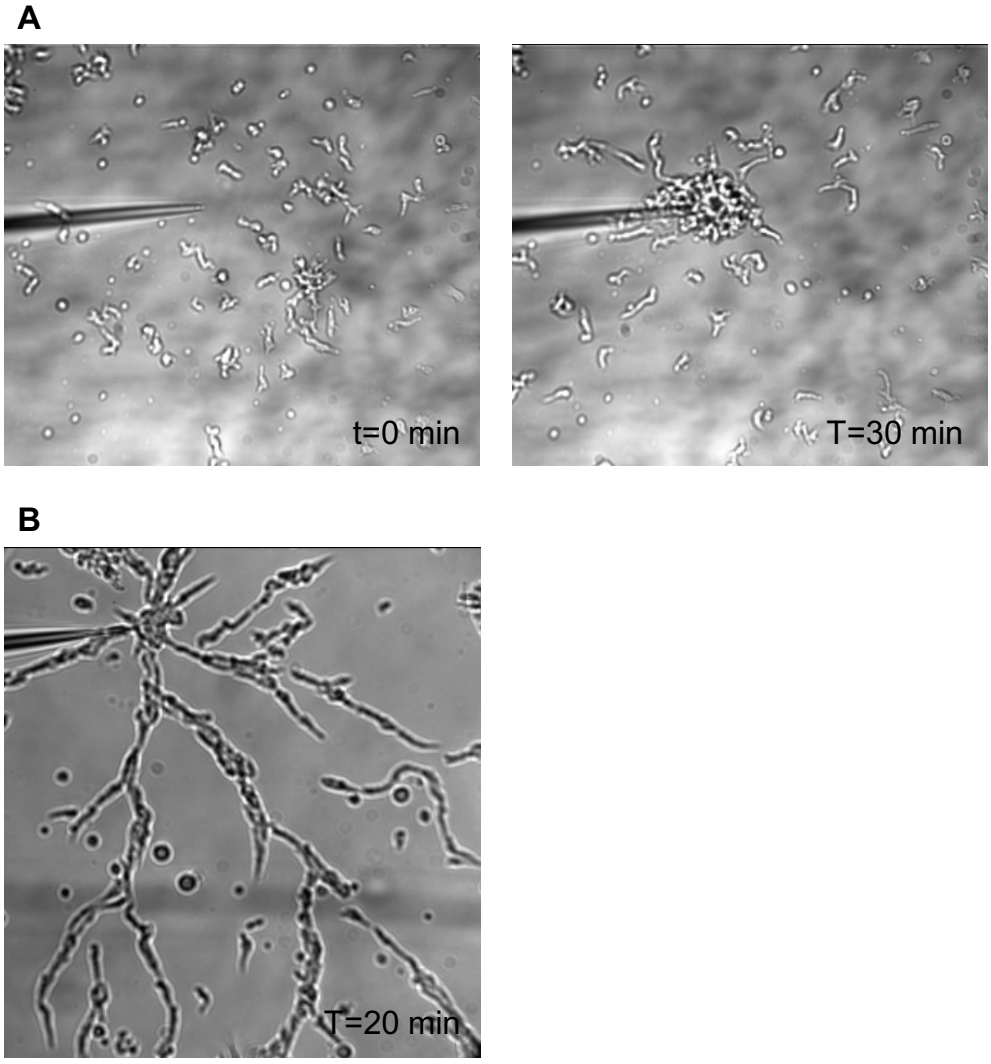

Figure 4.10: *rasC*$^{-}$*/rasG*$^{-}$ cells show directional movement upon expression of cAR1.